

Study of Photoconductivity and Photoluminescence in ZnO Microstructures Synthesized by Thermal Decomposition of Zinc Nitrate

Ravi S. Saxena¹ · Rajneesh K. Srivastava¹ · S. K. Mishra² · R. K. Shukla²

Received: 18 November 2014/Revised: 1 August 2016/Accepted: 15 November 2016/Published online: 5 December 2016
© The National Academy of Sciences, India 2016

Abstract In the present work, ZnO microstructures are synthesized by thermal decomposition of zinc nitrate $[\text{Zn}(\text{NO}_3)_2 \cdot 6\text{H}_2\text{O}]$ in air at 500 °C for 3 h. Structural and morphological study of ZnO microstructures have been analyzed by X-ray diffraction and scanning electron microscopy. UV–Vis absorption spectroscopy of ZnO microstructures exhibits absorption edge at 381 nm. Room temperature photoluminescence spectrum exhibits strong ultraviolet emission together with feeble visible emissions. In photoconductivity study, rise and decay of photocurrents under UV–Vis illumination have been recorded in air as well as in vacuum. Trap depth is calculated using decay portion of the rise and decay of photocurrent.

Keywords Photoconductivity · Photoluminescence · XRD · ZnO

1 Introduction

With wide band gap of ~ 3.37 eV and large exciton binding energy of ~ 60 meV at room temperature, zinc oxide (ZnO), a II–VI semiconducting material, is very promising for optoelectronic device applications e.g. solar cells, gas sensors, piezoelectric nanogenerators, photodetectors, UV light emitters [1–5] etc. Photoconductivity, the increase in the electrical conductivity of certain materials

when they are exposed to light of sufficient energy, serves as a tool to understand the internal processes in these materials, and it is also widely used to detect the presence of light and measure its intensity in light sensitive devices [6, 7]. Photoconductivity occurs when light is absorbed in the process of creating free carriers by intrinsic or extrinsic optical absorption. A good photoconductive device requires not only efficient charge separation but also efficient transport of charge carriers to electrodes. Mollow studied photoconductivity in ZnO single crystals [8]. Even relatively small concentration of native point defects and impurities significantly affect the electrical and optical properties of ZnO.

Generally, ZnO exhibits n-type semiconducting nature because of oxygen vacancies and other native defects such as interstitial Zn ions acting as donors [9]. In addition, the presence of these native defects is believed to be responsible for visible luminescence and photoconductivity (PC) in ZnO. A good photosensitive material should show a large and fast change in conductivity. Photoconductivity properties of ZnO have been investigated by several researchers [10–17]. The synthesis of ZnO nano and microstructures has potential applications in nano and microscale optoelectronic devices. Methods used for synthesis of ZnO nano and microstructures include hydrothermal method, electrochemical route, combustion method and thermal decomposition method [18–21]. Thermal decomposition method is a simple, inexpensive, reproducible and mass-scale yield method for the synthesis of ZnO microstructures, in which zinc nitrate as precursor to synthesize ZnO thin films and microstructures has been reported by Bacaksiz et al. [22], because zinc nitrate as a precursor has low solubility, low decomposition temperature and non requirement of any catalyst [23].

✉ Rajneesh K. Srivastava
rkumarsau@gmail.com

¹ Department of Electronics and Communication, University of Allahabad, Allahabad 211002, India

² Department of Physics, University of Lucknow, Lucknow 226007, India

In the present work, ZnO microstructures have been synthesized by thermal decomposition of zinc nitrate at 500 °C for 3 h. ZnO microstructures have been characterized for their structural properties by XRD as well as SEM and optical properties by UV–Vis as well as PL spectroscopy. Further, ZnO microstructures have been characterized for their photoconductivity properties by observing variation of darkcurrent and photocurrent with applied voltage and by recording the rise and decay of photocurrents in air as well as in vacuum.

2 Experimental Section

2.1 Chemicals

Zinc-nitrate $\text{Zn}(\text{NO}_3)_2 \cdot 6\text{H}_2\text{O}$ (purity: 99%, E. Merck Ltd.) was used as a precursor to synthesize ZnO microstructures directly without any special treatment.

2.2 Sample Preparation

In a typical procedure, about 2 g of $\text{Zn}(\text{NO}_3)_2 \cdot 6\text{H}_2\text{O}$ was placed into a crucible and was calcined at 500 °C for 3 h in a muffle furnace. ZnO microstructures were obtained in powder form.

2.3 Instrumentation

The structural, morphological and optical properties of ZnO comprising microstructures were investigated by X-ray diffraction (XRD) (PANalytical system, Cu $K\alpha$ radiation), scanning electron microscopy (SEM) (JEOL scanning electron microscope), UV–visible absorption spectroscopy (Perkin Elmer LS-35 spectrometer) and photoluminescence (PL) spectroscopy (Perkin Elmer LS-55 fluorescence spectrometer). For UV–Vis absorption spectroscopy the powder was dispersed in distilled water and stirred vigorously for homogeneous dispersion. In PL characterization, He–Ne laser as a source was used to excite the samples with excitation wavelength at 325 nm. For studying photoconductivity properties at room temperature, cell is formed by putting a thick layer of powdered sample in between two Cu electrodes with a spacing of 1 mm and area of illumination as 0.25 cm². Hg lamp of 300 W is used as UV–Vis light source. A stabilized dc field (50 V/cm to 500 V/cm) is applied across the cell. The rise and decay of photocurrent was recorded in air as well as in vacuum (10^{-3} mm of Hg to create oxygen-deficient ambient in a glass chamber with the help of Tarson Rockyvac 300 vacuum pump) using RISH Multi-18S with adapter RISH Multi SI-232.

3 Results and Discussion

3.1 Structural Study

Figure 1 shows X-ray diffraction (XRD) pattern of ZnO microstructures prepared by thermal decomposition of zinc nitrate at 500 °C for 3 h. The prominent peaks (100), (002), (101), (102), (110) and (103) are observed at $2\theta = 31.93^\circ$, 34.46° , 36.33° , 47.68° , 56.66° and 63.11° respectively. All diffraction peaks can be indexed to ZnO wurtzite structure corresponding to JCPDS card No. 36-1451. Similar results have been reported by Baskoutas et al. [24]. No other characteristic peaks of impurities such as Zn and $\text{Zn}(\text{OH})_2$ are observed, indicating that ZnO has been successfully synthesized. Peaks are sharper and narrower that indicates synthesized ZnO microstructures are of good crystalline structure. The lattice parameters in case of wurtzite phase are calculated using following formula:

$$\frac{1}{d_{hkl}^2} = \frac{h^2 + k^2}{a^2} + \frac{l^2}{c^2} \quad (3.1)$$

where $a = b$ and c are lattice parameters, d_{hkl} is the interplanar separation corresponding to Miller indices h , k , l . The calculated values of lattice parameters a , b and c for synthesized ZnO microstructures regarding most prominent peak (101) are calculated as 1.675, 1.675 and 4.652 Å respectively.

3.2 Morphology Study

Figure 2 shows SEM images of the synthesized ZnO microstructures formed by thermal decomposition of zinc nitrate at 500 °C for 3 h. The aggregated morphology of

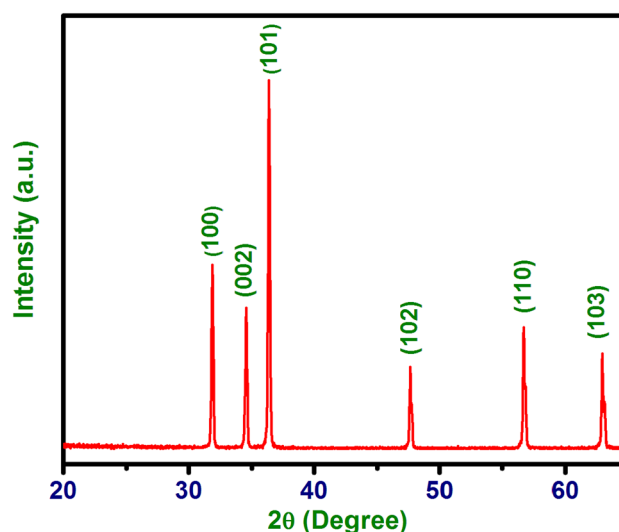
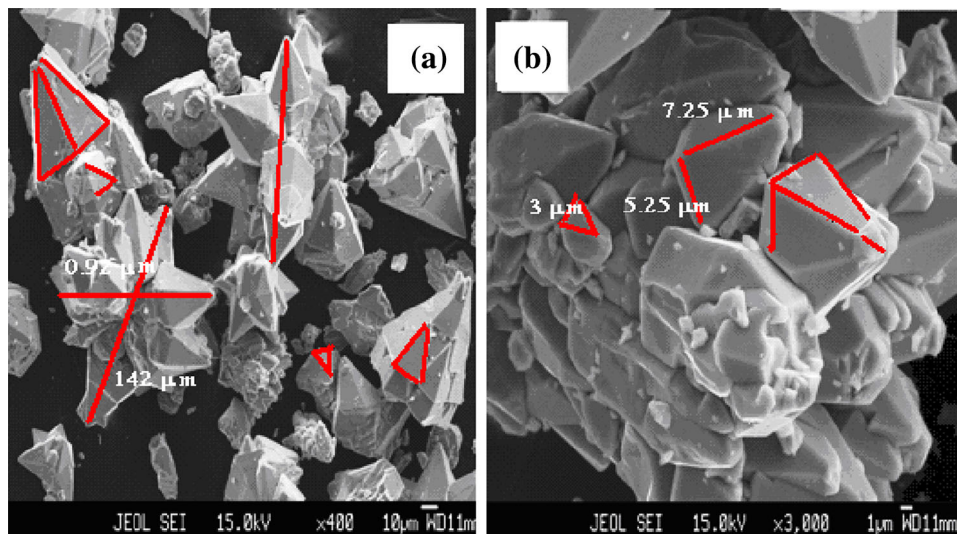


Fig. 1 X-ray diffraction (XRD) pattern of ZnO microstructures synthesized by thermal decomposition of zinc nitrate

Fig. 2 SEM images **a** at low magnification and **b** at high magnification of ZnO microstructures



six sided pyramid shaped microstructure has been observed. Flowerlike microstructures consist of six sided pyramid shaped microstructures. The six side surfaces and the base of the hexagonal micropylramids are smooth. Similar morphology has been reported by Ukewa et al. [25] for ZnO particles synthesized by decomposition of zinc nitrate hexahydrate. The average size of ZnO microstructures is around 125 μm which is higher than that reported by Ukewa et al. may be due to the fact that the thermal decomposition temperature 500 $^{\circ}\text{C}$ is higher than that used by Ukewa et al. [25].

3.3 UV–visible Absorption Study

Figure 3 shows UV–visible absorption spectrum of the sample ZnO microstructures showing an absorbance peak at 381 nm. Similar absorbance peak has been reported by Wa et al. [26] and Singh et al. [27].

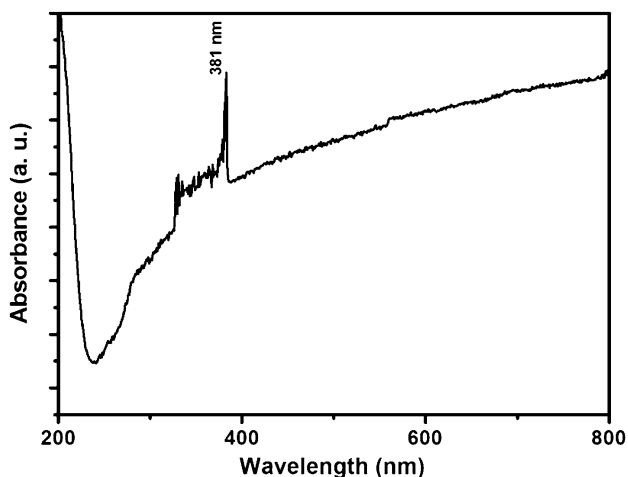


Fig. 3 Room temperature UV–visible absorption spectrum of ZnO microstructures

3.4 Photoluminescence Study

Figure 4 shows room temperature photoluminescence (PL) spectrum of the synthesized ZnO microstructure with wavelength of excitation as 325 nm at room temperature. The PL spectrum exhibit a strong UV emission peak at ~ 364 nm (3.39 eV) related to near band edge emission (NBE) of ZnO. This UV emission peak is attributed to recombination of free exciton– exciton collision process [28, 29].

3.5 Voltage Dependence of Photocurrent and Darkcurrent

Figure 6 shows the variation of dark-current (I_{dc}) and photocurrent (I_{pc}) under UV–Vis illumination with applied

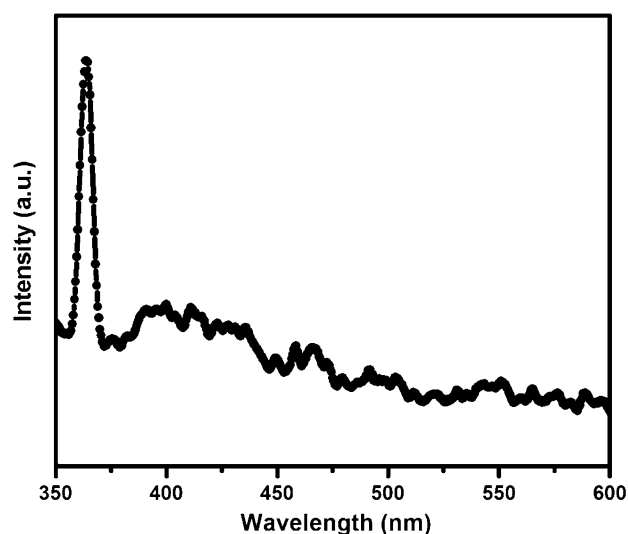


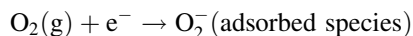
Fig. 4 Room temperature photoluminescence spectrum of ZnO microstructures

voltage in ZnO microstructures. In (I) versus $\ln(V)$ curves are straight lines having different slopes with respect to varying voltages according to power law, $I \propto V^r$, where r represents the slope of different straight line segments and I is either darkcurrent or photocurrent. Figure 5 shows that the dark current I_{dc} varies sublinearly ($r = 0.84$) at low voltages, and above 10 V, it varies superlinearly ($r = 1.25$), which may be due to flow of additional charge carriers being injected from one of the electrodes [7, 30, 31], and the variation of photocurrent (I_{pc}) with applied voltage is found to be superlinear that suggests that some charge carriers are being injected into the material from one of the electrodes [31–33].

3.6 Rise and Decay in Air and Vacuum

Figure 7 shows the rise and decay curve of photocurrent under UV–Vis Illumination with fix photo flux and bias voltage, measured in air as well in vacuum (10^{-3} mm of Hg pressure).

The cell was initially kept in dark till the dark current was stabilized. In air when the light was switched on, the photocurrent increased very fast due to quick generation of electron and hole pairs as a result of absorption of photons. After attaining a peak, the photocurrent started to decrease slowly even during steady illumination. This kind of anomalous behavior is attributed to the slow process of photoinduced chemisorption of oxygen molecules on the surface of ZnO microstructures [12, 34, 35]. Oxygen molecules get adsorbed on the surface as follows.



When the light was switched off the current decrease

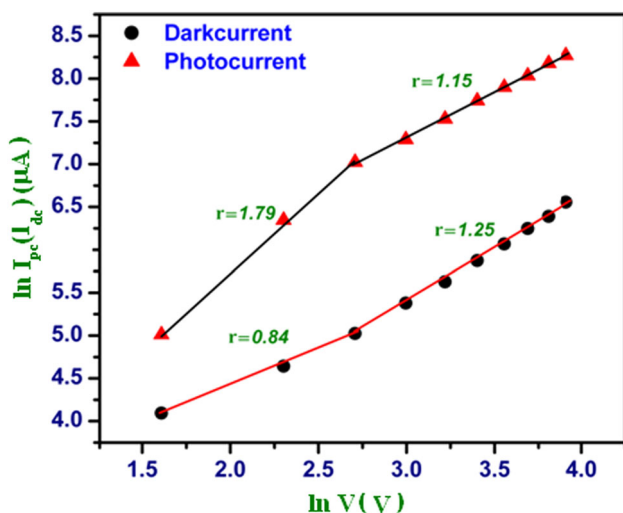
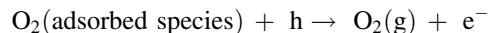


Fig. 5 Variation of photocurrent and darkcurrent as a function of applied voltage for ZnO microstructures

very fast initially, which could be attributed to recombination of free electron and holes [6, 36]. Later the current decreases slowly, which could be attributed to slow process of desorption of oxygen molecules as follows:



The rise and decay curve of photocurrent in vacuum is also shown in Fig. 6. In vacuum, no anomalous behavior was observed unlike that observed in air. This may be attributed to deficiency of oxygen molecules to be readsorbed on the surface of microstructures [37]. When light was switched on, the photocurrent increased sharply due to generation of electron hole pairs as a result of absorption of photons and then it increased slowly. After attaining the peak value the photocurrent got stabilized. The slow rise and decay in vacuum may not be attributed to decreased interfacial process in O_2^- deficient ambient [38].

Trap depth is calculated from the exponential decay portion of the rise and decay curves. Decay is expressed as follows [34, 39]:

$$I = I_0 \exp(-pt) \tag{3.2}$$

where, p is the probability of escape of an electron from the trap per second, I_0 is the current at the time when light is switched off and I is photocurrent at time t after the light is switched off. The probability of an electron escaping from a trap is also given by

$$p = S \exp(-E/kT) \tag{3.3}$$

where, k is Boltzman constant (1.381×10^{-23} J/K), T is absolute temperature and S is the frequency factor i.e. attempt to escape frequency [7, 40]. The attempt to escape frequency (S) is defined as the number per second that the quanta from crystal vibrations (phonons) attempt to eject

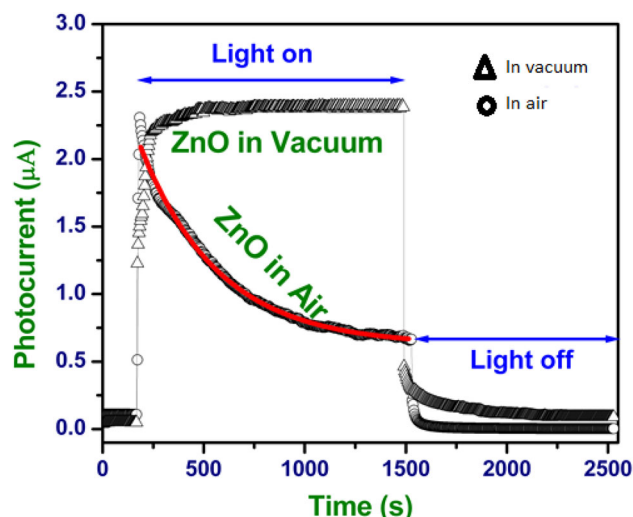


Fig. 6 Rise and decay curves in ZnO microstructures in air and well as in vacuum

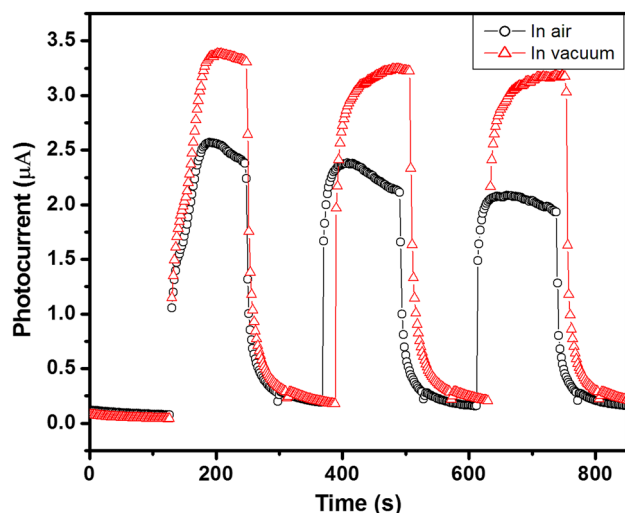


Fig. 7 Rise and decay under the periodic (2 min) illumination of ZnO microstructures in air as well as in vacuum

electrons from the traps, multiplied by the probability of transition from trap to conduction band. S is of the order of 10^9 at room temperature [41]. From the above equations, trap depth (E) becomes:

$$E = kT \left[\ln S - \ln \frac{\ln(I_o/I)}{t} \right] \quad (3.4)$$

The trap depth is calculated to be 0.59 and 0.67 eV for air and vacuum respectively.

Photocurrent transients were measured by illuminating the sample under the periodic pulses of UV–Vis illumination, at a fixed bias voltage of 20 V in air as well in vacuum (Fig. 7). The photocurrent transient cycles show that the photocurrents peak in air reduces in each cycle, which may be due to increased rate of recombination as a result of anomalous behavior of photocurrents in air [42]. Rise and decay times are of the order of few tens of seconds. Rise time lies in the range of 5–41 s whereas decay time is found to lie in the range of 19–28 s.

4 Conclusions

Thermal decomposition of zinc nitrate ($\text{Zn}(\text{NO}_3)_2 \cdot 6\text{H}_2\text{O}$) at 500 °C for 3 h yields wurzite ZnO microstructures of aggregated morphology of six sided pyramid particles. This method is simple, inexpensive, reproducible and mass yielding. Absorption edge is at 381 nm and PL spectrum exhibits a strong ultraviolet emission at ~ 364 nm together with four feeble visible emission bands. Photocurrent is found to vary superlinearly with applied voltage whereas variation of darkcurrent switches from sublinear to superlinear at high voltage. Anomalous behavior of photocurrent is observed in air wherein the photocurrent decreases even

during steady illumination which disappears in vacuum. Under periodic illumination of UV–Vis pulses, ZnO microstructures exhibit sufficiently fast switching transients, rise time lies in the range of 5–41 s whereas decay time is found to lie in the range of 19–28 s, that makes the synthesized ZnO microstructures good candidate for certain photo-switching devices.

Acknowledgements The authors are thankful to N.C.E.M.P, University of Allahabad, Allahabad for providing XRD and SEM facilities. S.K.M is grateful to UGC New Delhi for providing financial assistance under Dr. D. S. Kothari Post-Doctoral Fellowship [Ref. No. F.4-2/2006 (BSR)/13-764/2012 (BSR)].

References

- Bernede JC, Berredjem Y, Cattin L, Morsli M (2012) Improvement of organic solar cell performances using a zinc oxide anode coated by an ultrathin metallic layer. *Appl Phys Lett* 92:083304-3
- Spencer MJS (2012) Gas sensing applications of 1D-nanostructured zinc oxide: insights from density functional theory calculations. *Prog Mater Sci* 57(3):437–486
- Lu M, Song J, Lu MY, Chen M, Gao Y, Chen LJ, Wang ZL (2009) Piezoelectric nanogenerator using p-type ZnO nanowire arrays. *Nano Lett* 9(3):1223–1227
- Chang S, Chen KJ (2012) Zinc oxide nanoparticle photodetector. *J Nanomater*. doi:10.1155/2012/602398
- Kong YC, Yu DP, Zhang B, Fang W, Feng SQ (2001) Ultraviolet-emitting ZnO nanowires synthesized by a physical vapor deposition approach. *Appl Phys Lett* 78:407–409
- Bube RH (1967) Photoconductivity of solids. Wiley, New York
- Mishra SK, Srivastava RK, Prakash SG, Yadav RS, Panday AC (2010) Photoluminescence and photoconductive characteristics of hydrothermally synthesized ZnO nanoparticles. *Opto Electron Rev* 18(4):467–473
- Mollow E (1954) Photoconductivity. Co & ed RG Breckenridge. Wiley, New York
- Janotti A, Van de Walle CG (2009) Fundamentals of zinc oxide as a semiconductor. *Rep Prog Phys* 72:126501–126529
- Pandey N, Srivastava RK, Prakash SG (2013) Study of dark conductivity and photoconductivity in dysprosium doped zinc oxide synthesized by heat treatment method. *Nat Acad Sci Lett* 36(5):521–526
- Polyakov AY, Smirnov NB, Govorkov AV, Kozhukhova EA, Pearton SJ, Norton DP, Osinsky A, Dabiran A (2006) Electrical properties of undoped bulk ZnO substrates. *J Electron Mater* 35(4):663–669
- Krunks M, Dedova T, OjaAcik I (2006) The effects of zinc nitrate, zinc acetate and zinc chloride precursors on investigation of structural and optical properties of ZnO thin films. *Thin Solid Films* 515(3):1157–1160
- Yadav HK, Gupta V (2012) A comparative study of ultraviolet photoconductivity relaxation in zinc oxide (ZnO) thin films deposited by different techniques. *J Appl Phys* 111:102809–102814
- Takahashi Y, Kanamori YM, Kondoh A, Minoura H, Ohya Y (1994) Photoconductivity of ultrathin zinc oxide films. *Jpn J Appl Phys* 33:6611–6615
- Zhang DH, Brodie DH (1995) Photoresponse of polycrystalline ZnO films deposited by r.f. bias sputtering. *Thin Solids Films* 261(1):334–339

16. Yadav HK, Sreenivas K, Gupta V (2010) Study of metal/ZnO based thin film ultraviolet photodetectors: the effect of induced charges on the dynamics of photoconductivity relaxation. *J Appl Phys* 107(4):4507-04
17. Yadav HK, Sreenivas K, Gupta V (2010) Persistent photoconductivity due to trapping of induced charges in Sn/ZnO thin film based UV photodetector. *Appl Phys Lett* 96:3507–3522
18. Maeda K, Sato M, Niiikura I, Fukuda T (2005) Growth of 2 inch ZnO bulk single crystal by the hydrothermal method. *Semicond Sci Technol* 20:S49–S54
19. Ding L, Zhang R, Fan L (2013) Electrochemical route to the synthesis of ZnO microstructures: its nestlike structure and holding of Ag particles. *Nanoscale Res Lett* 8(78):1–7
20. Lin CS, Hwang CC, Lee WH, Tong WY (2007) Preparation of zinc oxide (ZnO) powders with different types of morphology by a combustion synthesis method. *Mater Sci Eng B* 140(25):31–37
21. Benard P, Auffredic JP, Louër D (1994) A study of the thermal decomposition of ammine zinc hydroxide nitrates. *Thermochim Acta* 232:65–76
22. Bacaksiz E, Parlak M, Tomakin M, Ozeclik A, Karakız M, Altunbas M (2008) The effects of zinc nitrate, zinc acetate and zinc chloride precursors on investigation of structural and optical properties of ZnO thin films. *J Alloy Compd* 466:447–450
23. Radzimska AK, Jesionowski T (2014) Zinc oxide from synthesis to application: a review. *Materials* 7:2833–2881
24. Baskoutas S, Giabouranis P, Yannopoulos SN, Dracopoulos V, Toth L, Chrissanthopoulos A, Bouropoulos N (2007) Preparation of ZnO nanoparticles by thermal decomposition of zinc alginate. *Thin Solid Films* 515:8461–8464
25. Uekawa N, Kojima T, Kakegawa K (2009) Synthesis of nitrogen-doped ZnO particles by decomposition of zinc nitrate hexahydrate in molten ammonium salts. *J Mater Res* 24(11):3343–3349
26. Wa L, Wang X, Yan S, Yu H, Li Z, Zou Z (2012) ZnO plates synthesized from the ammonium zinc nitrate hydroxide precursor. *Cryst Eng Comm* 14:154–159
27. Singh S, Thiyagarajan P, Kant KM, Anita D, Thirupathiah S, Rama N, Tiwari B, Kottaisamy M, Ramachandra Rao MS (2007) Structural and physical properties of ZnO based materials in various forms: bulk, thin film and nano. *J Phys D Appl Phys* 40:6312–6327
28. Vanheusden K, Warren WL, Seager CH, Tallant DR, Voigt JA, Gnade BE (1996) Mechanisms behind green photoluminescence in ZnO phosphor powders. *J Appl Phys* 79:7983–7990
29. Mishra SK, Bayan S, Chakraborty P, Srivastava RK (2014) Defect-dominated optical emission and enhanced ultraviolet photoconductivity properties of ZnO nanorods synthesized by simple and catalyst free approach. *Appl Phys A* 115(4):1193–1203
30. Rose A (1951) An outline of some photoconductivity process. *RCA Rev* 12:362–414
31. Devi S, Prakash SG (1994) Photoconductivity studies of composites. *J Phys* 43:245–253
32. Smith RW, Rose A (1955) Space-charge-limited currents in single crystals of cadmium sulfide. *Phys Rev* 97:1531–1538
33. Pillai PKC, Shroff N, Kumar NN, Tripathi AK (1985) Photoconductivity and dark conductivity studied of CdS_{1-x}Se_x(Cu) sintered layers. *Phys Rev B* 32:8228–8233
34. Mishra SK, Bayan S, Shankar R, Chakraborty P, Srivastava RK (2014) Enhanced vacuum photoconductivity of chemically synthesized ZnO nanostructures. *Philos Mag* 94(9):914–924
35. Bera A, Basak D (2009) Effect of surface capping with poly(vinyl alcohol) on the photocarrier relaxation of ZnO nanowires. *Appl Mater Interfaces* 1(19):2066–2070
36. Bube RH (1992) Photoelectronic properties of semiconductors. Cambridge University Press, New York
37. Ahn SE, Ji HJ, Kim K, Kim GT, Bae CH, Park SM, Kim YK, Ha JS (2007) Origin of the slow photoresponse in an individual sol-gel synthesized ZnO nanowire. *Appl Phys Lett* 90:153106-3
38. Bera A, Basak D (2009) Role of defects in the anomalous photoconductivity in ZnO nanowires. *Appl Phys Lett* 94:163119-3
39. Shankar R, Srivastava RK, Prakash SG (2013) Study of dark-conductivity and photoconductivity of ZnO nano structures synthesized by thermal decomposition of zinc oxalate. *Electron Mater Lett* 9(5):555–559
40. Bhushan S, Diwan D (1984) Photoconductivity of ZnO phosphors. *Natl Acad Sci Lett* 7:12–16
41. Randall JF, Wilkins JHF (1945) Phosphorescence and electron traps the study of trap distributions. *Proc R Soc A* 184:366–389
42. Vomvas A, Pomoni K, Trapalis C, Todorova N (2007) Photoconductivity in sol-gel TiO₂ thin films with and without ammonia treatment. *Mater Sci Pol* 25(3):809–816